Shiftless inhibits flavivirus replication in vitro and is neuroprotective in a mouse model of Zika virus pathogenesis

Natasha W. Hanners[a], Katrina B. Mar[b,1], Ian N. Boys[c,1], Jennifer L. Eitson[b], Pamela C. De La Cruz-Rivera[b], R. Blake Richardson[b], Wenchun Fan[b], Mary Wight-Carter[d], and John W. Schoggins[b,2]

[a]Department of Pediatrics, University of Texas Southwestern Medical Center, Dallas, TX 75390; [b]Department of Microbiology, University of Texas Southwestern Medical Center, Dallas, TX 75390; [c]Department of Immunology, University of Texas Southwestern Medical Center, Dallas, TX 75390; and [d]Animal Resource Center, University of Texas Southwestern Medical Center, Dallas, TX 75390

Edited by Stephen P. Goff, Columbia University Irving Medical Center, New York, NY, and approved October 29, 2021 (received for review June 17, 2021)

Flaviviruses such as Zika virus and West Nile virus have the potential to cause severe neuropathology if they invade the central nervous system. The type I interferon response is well characterized as contributing to control of flavivirus-induced neuropathogenesis. However, the interferon-stimulated gene (ISG) effectors that confer these neuroprotective effects are less well studied. Here, we used an ISG expression screen to identify Shiftless (SHFL, C19orf66) as a potent inhibitor of diverse positive-stranded RNA viruses, including multiple members of the *Flaviviridae* (Zika, West Nile, dengue, yellow fever, and hepatitis C viruses). In cultured cells, SHFL functions as a viral RNA-binding protein that inhibits viral replication at a step after primary translation of the incoming genome. The murine ortholog, Shfl, is expressed constitutively in multiple tissues, including the central nervous system. In a mouse model of Zika virus infection, *Shfl*$^{-/-}$ knockout mice exhibit reduced survival, exacerbated neuropathological outcomes, and increased viral replication in the brain and spinal cord. These studies demonstrate that Shfl is an important antiviral effector that contributes to host protection from Zika virus infection and virus-induced neuropathological disease.

flaviviruses | pathophysiology | neurotropic viruses | type I interferon

Flavivirus infections contribute a significant human health burden. Historically prominent flaviviruses such as dengue (DENV) and yellow fever virus (YFV) have infected millions of humans, with DENV being responsible for 100 million symptomatic cases yearly and YFV causing 130,000 severe cases yearly (1). In addition, emerging and reemerging viruses cause periodic but potentially devastating outbreaks. Of particular concern are neurotropic flaviviruses, which may cause lifelong sequelae and disability even in survivors. Neurologic manifestations of flavivirus infections include Guillain–Barré syndrome, microcephaly and congenital Zika syndrome (CZS), meningoencephalitis, and acute flaccid paralysis. In 1999, West Nile virus (WNV) emerged in North America, and in 2012 alone, 5,674 cases were diagnosed in the United States, of which 51% were neuroinvasive (2). The 2015 to 2016 reemergence of Zika virus (ZIKV) and microcephaly devastated many Latin American countries, and the impact of CZS is still manifesting. While these outbreaks are currently quiescent, the timing of reemergence or the potential for flaviviruses such as Usutu or Powassan to emerge and cause epidemics is unknown.

Despite the severe pathologic consequences noted above, most flavivirus infections in humans do not result in life-threatening disease, in large part due to a highly effective immune system that controls viral replication and thus limits pathology. Host immune responses to flaviviruses are mediated by both innate and adaptive immune responses, with the interferon (IFN) response providing critical protection against these viruses (3–9). The IFN response controls viral infection in part through the action of interferon-stimulated gene (ISG) products, many of which have direct antiviral effector activities. Of the hundreds of known human ISGs, a small number have been shown to inhibit flaviviruses, including CH25H, IFIT2, IFITM3, IFI6, OAS1/RNaseL, PKR, RTP4, TRIM5-α, and viperin (6, 7, 10–18). For some of these effectors, insight into mechanisms of action has been obtained, and several have been validated as antiflavivirus effectors by gene knockout (KO) in vivo. The mouse ISGs that have been knocked out and tested in flavivirus pathogenesis models include *Ifit2*, *Ifi27l2a*, *Ifitm3*, *Oas1b*, *Rnasel*, *Pkr*, and *viperin* (6, 19–24). In this study, we examine the role of another ISG, Shiftless (SHFL, formerly C19orf66) that has been shown in previous studies to inhibit diverse viruses in cell culture, including neurotropic flaviviruses (25–28). We present a cell-based ISG screen that identifies SHFL as antiviral against multiple positive-strand RNA viruses. We demonstrate that SHFL targets viral replication at a step after primary translation of the incoming viral genome. We additionally used *Shfl* KO mice to demonstrate that this effector has neuroprotective effects in a ZIKV pathogenesis model.

Significance

Flaviviruses are significant human pathogens and emerging infectious disease threats. A screen of interferon-inducible genes revealed Shiftless (SHFL) as a potent antiviral effector, inhibiting all *Flaviviridae* tested, including West Nile, Zika, dengue, yellow fever, and hepatitis C viruses. Mechanistic studies showed that SHFL inhibits viral replication at a point after translation of the incoming genome. In whole-body *Shfl* knockout (KO) mice, compared to wild-type mice, the *Shfl* KO mice were more susceptible to Zika virus. Notably, *Shfl* was uniquely required for controlling replication in the brain and spinal cord, demonstrating an unappreciated neuroprotective role for this effector in vivo. SHFL is a key antiviral effector that specifically inhibits flavivirus genome replication, and *Shfl* protects mice from Zika virus–induced neuropathogenesis.

Author contributions: N.W.H. and J.W.S. designed research; N.W.H., K.B.M., I.N.B., J.L.E., P.C.D.L.C.-R., R.B.R., W.F., and J.W.S. performed research; N.W.H., K.B.M., I.N.B., J.L.E., P.C.D.L.C.-R., R.B.R., W.F., M.W.-C., and J.W.S. analyzed data; and N.W.H. wrote the paper.

The authors declare no competing interest.

This article is a PNAS Direct Submission.

[1]K.B.M. and I.N.B. contributed equally to this work.

[2]To whom correspondence may be addressed. Email: john.schoggins@utsouthwestern.edu.

This article contains supporting information online at http://www.pnas.org/lookup/suppl/doi:10.1073/pnas.2111266118/-/DCSupplemental.

Published December 3, 2021.

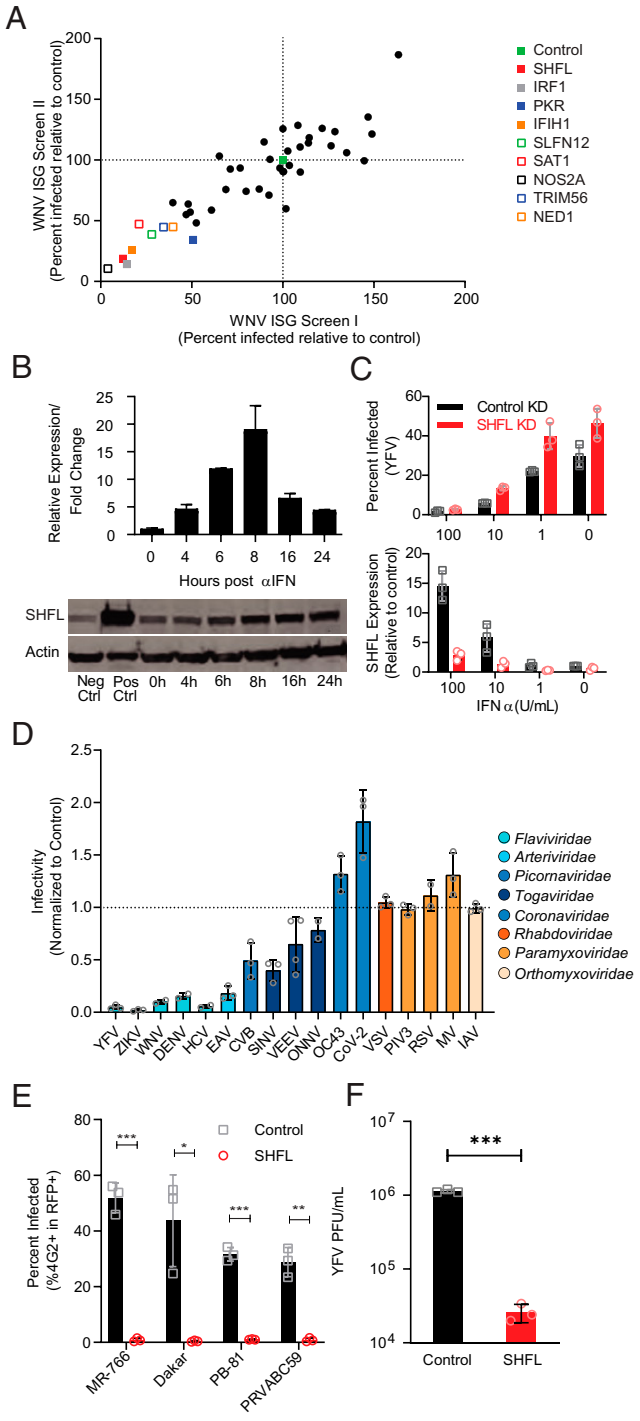

Fig. 1. SHFL is an ISG that suppresses the *Flaviviridae*. (*A*) Cells coexpressing an ISG and RFP were infected with WNV-GFP. Plotted are the mean percentages of GFP-positive (virally infected) in RFP-positive (ISG-expressing) cells of two biologic replicates (Screen I, *x*-axis and Screen II, *y*-axis), relative to control (Fluc). (*B*) SHFL expression in IFN-treated (100 U/mL) Huh7.5 cells as assessed by qRT-PCR (*Top*) and Western blot (*Bottom*). (*C*) YFV-17D-Venus infectivity as assessed by flow cytometry (*Top*) in IFN-treated U2OS cells pretreated with siRNA targeting SHFL or a nonsilencing control, with SHFL expression assessed by qRT-PCR (*Bottom*). (*D*) Infectivity of diverse viruses in cells stably expressing SHFL or vector control, quantified by flow cytometry. (*E*) Infectivity of ZIKV strains (MOI 1) in Huh7.5 cells stably expressing SHFL or empty vector control, quantified by flow cytometry. $*P < 0.05$; $**P < 0.01$; $***P < 0.001$. (*F*) Viral titers in supernatants of Huh7.5 cells stably expressing SHFL or control and infected with YFV-17D at MOI 0.1. Bars indicate the mean ± SD of $n = 2$ biological replicates (*D*: WNV, DENV, HCV, ONNV, RSV), $n = 3$ biological replicates (*B–D*: YFV, ZIKV, EAV, CVB, SINV, OC43, CoV2, VSV, PIV3, MV, and IAV; *E* and *F*), or $n = 4$ (*E*: VEEV).

Results

In previous screens to identify antiviral ISGs, we used lentiviral vectors for ISG delivery (11, 14, 29). However, 52 of the 387 genes in our library could not be efficiently packaged into lentiviral pseudoparticles. To assess the antiviral potential of these genes, we transiently transfected tissue culture cells with a plasmid coexpressing an ISG and a red fluorescent protein (RFP) in a one-gene to one-well format (*SI Appendix*, Table S1). Firefly luciferase (Fluc) and IRF1 were included as negative and positive controls, respectively. We infected ISG-expressing cells with a GFP-expressing WNV and measured infectivity in RFP-positive cells by flow cytometry. Several genes known to have antiviral activity when ectopically expressed were identified, including *EIF2AK2*, *IFIH1*, and *SAT1* (encoding PKR, MDA5, and spermidine/spermine N1-acetyltransferase 1, respectively). SHFL, a more recently identified antiviral ISG, also exhibited potent antiviral activity against WNV (Fig. 1*A* and *SI Appendix*, Table S1).

SHFL (formerly C19orf66, also named RyDEN, IRAV, FLJ11286) is a 291 amino acid protein that has been described as an antiviral ISG that inhibits replication of flaviviruses, alphaviruses, and retroviruses (25–28, 30, 31). SHFL is conserved as an ISG across mammals, and we confirmed it as an ISG in Huh7.5 human hepatoma cells (Fig. 1*B*) (32). To assess the role of SHFL as an IFN-induced antiviral gene, we used small interfering RNA (siRNA)-mediated gene silencing and found that the antiviral effects of IFN-α against YFV were partially abrogated in cells with reduced *SHFL* expression (Fig. 1*C*) (32). We next assessed antiviral specificity by screening a variety of positive-sense and negative-sense RNA viruses in cells ectopically expressing SHFL (Fig. 1*D*). We infected cells with positive-sense RNA viruses including the flaviviruses WNV, ZIKV, DENV, and YFV, the hepacivirus hepatitis C virus (HCV), the arterivirus equine arteritis virus (EAV), the picornavirus coxsackie B3 virus (CVB3), and the alphaviruses Venezuelan equine encephalitis virus (VEEV), Sindbis virus (SINV), and O'nyong'nyong virus (ONNV). SHFL expression suppressed each of these viral infections compared to control cells stably expressing an empty vector. SHFL most potently inhibited viruses of the *Flaviviridae* family, including WNV, YFV, DENV, and ZIKV, as well as the related HCV. Other positive-sense RNA viruses EAV, CVB3, VEEV, SINV, and ONNV were inhibited, albeit to a lesser degree. SHFL did not inhibit the endemic human coronavirus OC43 (HCoV-OC43), the zoonotic coronavirus SARS-CoV-2, or five negative-sense RNA viruses, including vesicular stomatitis virus (VSV), parainfluenza virus 3 (PIV3), respiratory syncytial virus (RSV), measles (MV), or influenza virus (IAV). A strong antiviral phenotype was observed with ZIKV using a reporter MR766-Venus (Fig. 1*D*), and the phenotype was similar in nonreporter strains of African and Asian lineages, MR-766, Dakar 41519, Pernambuco (PB-81), and PRVABC59 (Fig. 1*E*). Additionally, in plaque assays, SHFL reduced YFV production by over 10-fold as compared to control cells (Fig. 1*F*).

We next sought to determine which viral replication step was inhibited by SHFL. We first performed an infection time course using a reporter HCV expressing Gaussia luciferase (Gluc) (HCV-Gluc). At early time points postinfection (4, 6, and 8 h), Gluc levels were similar in both control and SHFL-expressing cells, suggesting that early steps of viral entry and primary translation were not affected. Conversely, Gluc levels at later time points (24 and 48 h) were significantly reduced in SHFL-

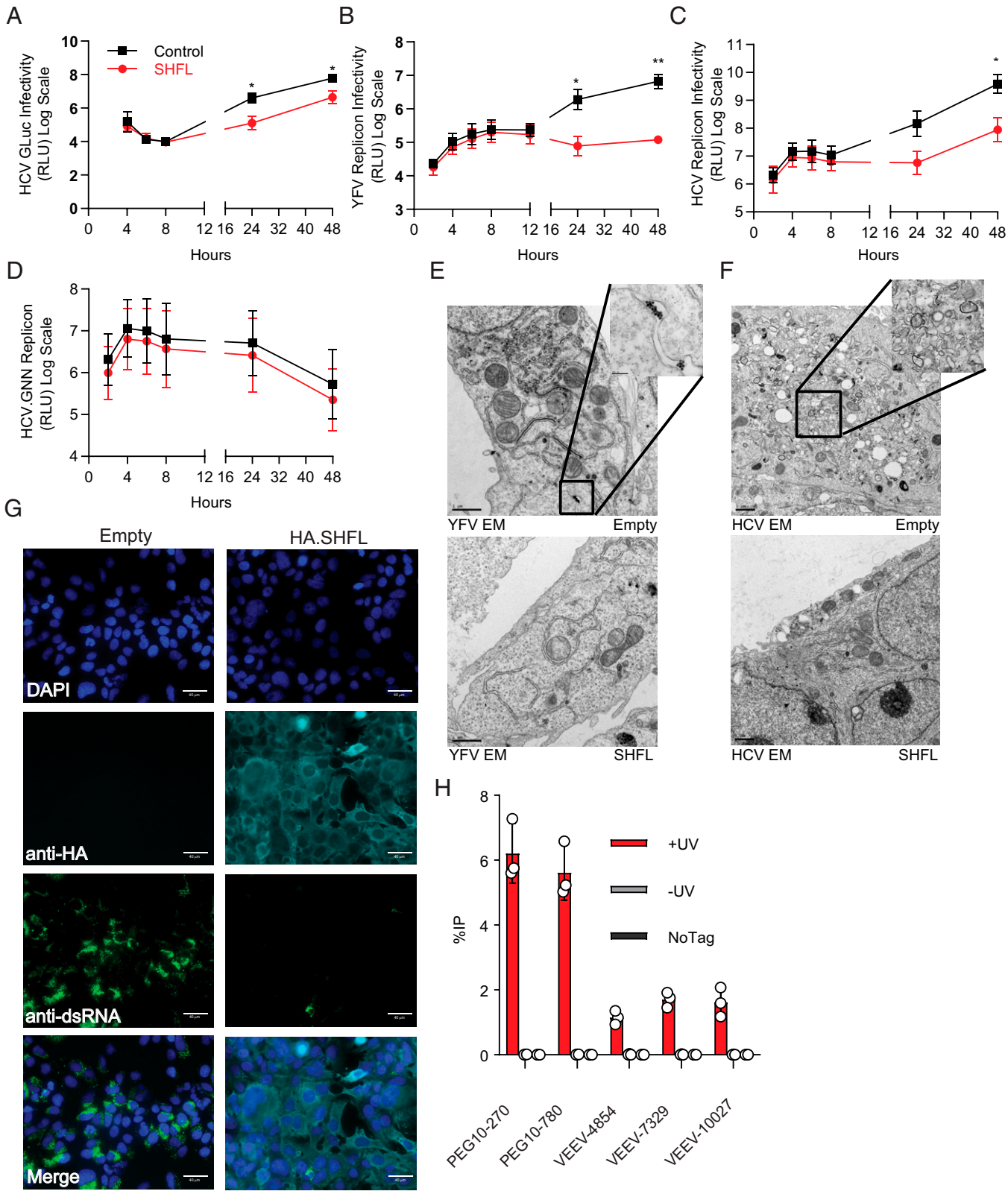

Fig. 2. SHFL inhibits the replication phase of the *Flaviviridae* and binds viral RNA. (*A*) Huh7.5 cells stably expressing SHFL or vector control and infected with HCV-Gluc. Supernatants were collected at time points shown and assessed by luciferase assay. (*B–D*) Huh7.5 cells stably expressing SHFL or vector control and transfected with (*B*) YFV replicon, (*C*) HCV replicon, or (*D*) polymerase-defective HCV (HCV-GNN). Cells were lysed, and the relative luciferase units (RLU) was assessed by luminometry. (*E* and *F*) Electron microscopic analysis of Huh7.5 cells stably expressing empty vector control (*Top* images) or SHFL (*Bottom* images) and infected with YFV (*E*) or HCV (*F*). Images are representative of 10 cells assessed per cell line per infection. (*G*) Huh7.5 cells stably expressing empty vector control or HA.SHFL and infected with YFV-17D at an MOI of 1. Cells were stained with anti-HA and anti-dsRNA antibodies. (*H*) *STAT1*$^{-/-}$ human fibroblasts stably expressing HA-tagged SHFL or vector control were infected with VEEV at an MOI of 10 for 16 h. +UV, ultraviolet (UV)–cross-linked HA.SHFL cells; −UV, non–cross-linked HA.SHFL cells; NoTag, UV–cross-linked vector control cells. Bars indicate the mean ± SD of $n = 3$ biological replicates (*A–C* and *H*), $n = 2$ (*D*), and $n = 2$ with representative images shown (*E–G*). *P < 0.05; **P < 0.01.

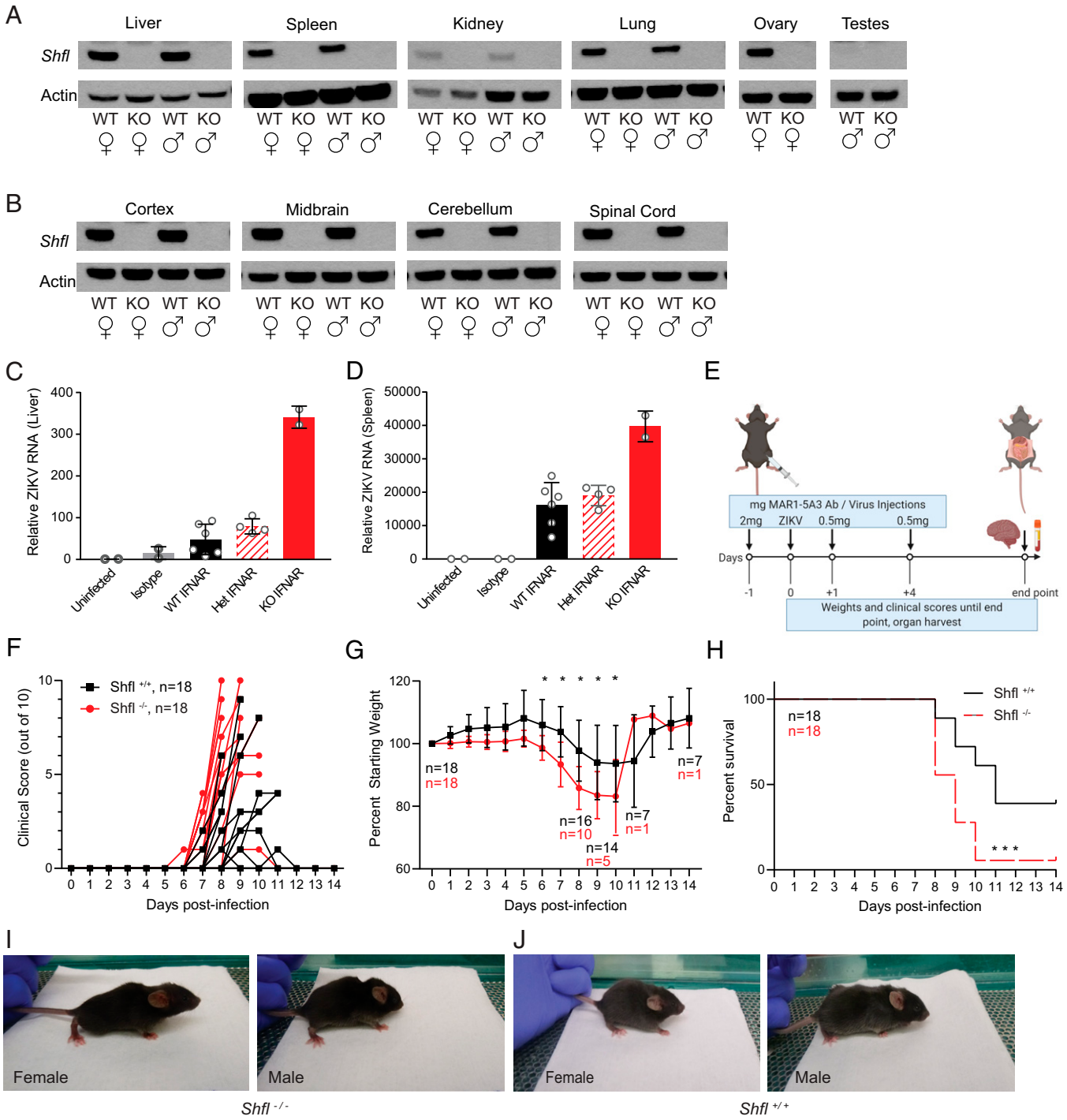

Fig. 3. Loss of SHFL ortholog *Shfl* results in increased morbidity and mortality in a mouse model of ZIKV pathogenesis. (*A* and *B*) Shfl protein expression in wild-type (WT) and KO mice. (*C* and *D*) $Shfl^{+/+}$, $Shfl^{+/-}$, and $Shfl^{-/-}$ mice infected with 500 pfu MR766 ZIKV. Viral RNA levels were assessed by qRT-PCR in liver (*C*) and spleen (*D*). (*E*) Experimental procedure for pathogenesis studies. (*F–H*) Clinical scores (*F*), weight loss (*G*), and survival (*H*) in ZIKV-infected mice. Data represent two independent experiments, $n = 9$ mice per genotype per experiment. (*I* and *J*) Images showing kyphosis and ruffled fur of infected $Shfl^{-/-}$ (*I*) or $Shfl^{+/+}$ (*J*) mice. Statistical analysis of weight loss was done using unpaired *t* test with Holm–Šídák correction for multiple comparisons. For *G*, the asterisks correspond to the following *P* values: Day 6 (D6), $P = 0.023$; D7 to 8, $P < 0.001$; D9, $P = 0.003$; and D10, $P = 0.049$. Statistical analysis of survival was done using log-rank Mantel–Cox test, $P < 0.001$.

expressing cells compared to control cells (Fig. 2*A*). This suggests SHFL may target viral genome replication. We next used YFV or HCV "subgenomic replicons" to further examine the impact of SHFL on viral replication. Subgenomic replicons are viral RNA genomes expressing Renilla luciferase (Rluc) or Gluc in place of structural protein genes. When transfected into cells, the naked viral RNA bypasses canonical viral entry routes, replicates, and expresses luciferase in a manner that temporally distinguishes primary viral RNA translation from genome amplification. A YFV-Rluc replicon (Fig. 2*B*) and HCV-Gluc replicon (Fig. 2*C*) were inhibited by SHFL at later stages of replication but not early stages of primary translation.

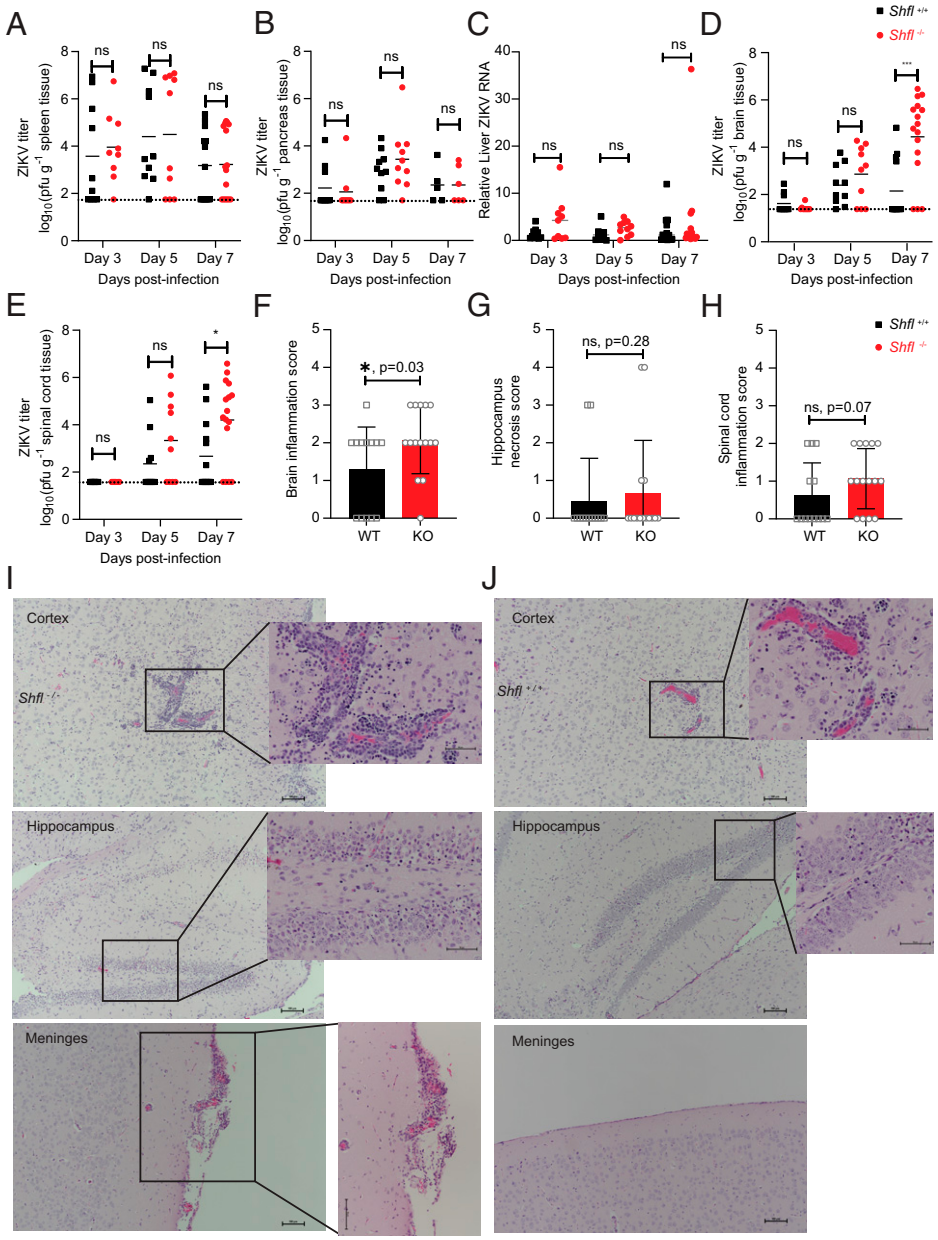

Fig. 4. Loss of *Shfl* in mice promotes increased ZIKV dissemination and pathology in the CNS. (*A*–*E*) Viral titers in spleen (*A*), pancreas (*B*), liver (*C*), brain (*D*), and spinal cord (*E*) in infected $Shfl^{+/+}$ and $Shfl^{-/-}$ mice quantified by plaque assay (*A*, *B*, *D*, and *E*) or qRT-PCR (*C*). (*F*–*J*) Histopathology of CNS tissues. Inflammation/necrosis scores in brain (cerebral cortex) (*F*), hippocampus (*G*), and spinal cord (*H*), and representative histopathology of $Shfl^{-/-}$ (*I*) and $Shfl^{+/+}$ (*J*) brains are shown. Regions shown are perivascular cerebral cortex, hippocampus, and meninges with squares denoting areas of inflammation (cortex and meninges) and cell death (hippocampus). Statistical analysis was done using unpaired *t* test with Holm–Šídák correction for multiple comparisons (*A*–*E*) or one-tailed Mann–Whitney *U* test (*F*–*H*). $n = 4$ to 9 mice/genotype/day postinfection assessed (D3, 5, 7 postinfection). $*P < 0.05$; $***P < 0.001$. ns, not significant.

To examine primary translation in the absence of replication, we used a polymerase-defective replicon, HCV-Gluc-GNN, and found no difference in luciferase production between SHFL-expressing and control cells (Fig. 2*D*). These results were further supported by electron microscopic analysis of Huh7.5 cells infected with YFV-17D (Fig. 2*E*) or HCV (Fig. 2*F*), revealing that SHFL-expressing cells had fewer viral replication organelles when compared to control cells. These replicon-based and electron microscopy studies corroborate similar findings recently reported by others and indicate that SHFL targets a viral replication step after primary translation of the incoming genome (27). Additionally, SHFL expression strongly inhibited viral double-stranded RNA (dsRNA), which is produced as an intermediate product of genome replication (Fig. 2*G* and *SI Appendix*, Fig. S1). Similar to previous studies, we also demonstrated that SHFL is an RNA-binding protein (25, 26). Using cross-linking immunoprecipitation (CLIP) paired with qPCR, we found that in VEEV-infected cells, SFHL binds both viral RNA and a known cellular target RNA, PEG10 (Fig. 2*H*).

We next questioned whether SHFL has an antiviral role in vivo. The *SHFL* mouse ortholog, *Shfl* (formerly *A230050P20Rik*), shares 93% amino acid identity with the human protein (*SI Appendix*, Fig. S2*A*), indicating it may have conserved antiviral function. We confirmed this by demonstrating that ectopically expressed Shfl inhibits YFV virus in 293T cells (*SI Appendix*, Fig. S2*B*). We next generated *Shfl* KO mice by crossing a C57BL/6J mouse bearing a reporter-tagged *Shfl* null allele (tm1) with a Cre-expressing mice (33). The resulting mice

express a lacZ reporter at the second exon of *Shfl*, resulting in a nonconditional KO of the gene (*SI Appendix*, Fig. S3 *A* and *B*). Loss of expression in several tissues was verified at the protein level (Fig. 3 *A* and *B* and *SI Appendix*, Figs. S3*C* and S4). To characterize the effects of a constitutive gene KO, breeding efficiency and outcomes were monitored. Phenotypically, $Shfl^{-/-}$ mice were normal in appearance and no physical deformities were noted in comparison to $Shfl^{+/+}$ mice (*SI Appendix*, Fig. S3*D*). $Shfl^{-/-}$ and $Shfl^{+/+}$ mice bred with roughly equal efficiency (*SI Appendix*, Table S2) and no breeding anomalies were noted. There was no apparent embryonic lethality with $Shfl^{+/-}$ crosses, as the proportion of genotypes approximated Mendelian inheritance (*SI Appendix*, Table S3).

Immunocompetent mice are intrinsically resistant to certain flaviviruses due to the inability of flavivirus NS5 to antagonize mouse STAT2 (34). This has necessitated the use of a partially immunosuppressed mouse model to achieve flavivirus infection with nonadapted viruses (35, 36). We established a similar model and demonstrated that a single administration of an anti-Ifnar1 antibody permitted replication of ZIKV in wild-type C57BL6/J. ZIKV RNA increased ∼3-fold in liver and 15,000-fold in spleen in these mice when compared to mice treated with isotype control antibody (Fig. 3 *C* and *D*). Genetic ablation of *Shfl* resulted in an additional 7-fold increase in viral RNA in liver and 2.5-fold increase in spleen, compared to $Shfl^{+/+}$ mice, suggesting that the mouse ortholog of SHFL restricts ZIKV infection in vivo. To improve viral infectivity and pathogenesis, we modified our antibody administration protocol based on a previously published study (Fig. 3*E*) (37). Mice were scored daily for condition of fur, activity, paralysis, posture, respiratory distress, and weight loss (*SI Appendix*, Table S4) until the experimental end point or humane euthanasia, at which point tissue and serum samples were obtained.

In $Shfl^{-/-}$ mice infected with ZIKV-Dakar 41519, clinical disease developed more rapidly and was more severe than in $Shfl^{+/+}$ mice (Fig. 3*F*). Infected $Shfl^{-/-}$ mice also lost significantly more weight compared to $Shfl^{+/+}$ after viral challenge. (Fig. 3*G*). Furthermore, nearly all $Shfl^{-/-}$ mice succumbed to ZIKV infection, whereas the infection was less lethal in $Shfl^{+/+}$ mice (Fig. 3*H*). At the point of humane euthanasia, typically around 7 to 8 d postinfection, $Shfl^{-/-}$ mice had decreased activity, more pronounced cachexia, kyphosis, and ruffled fur (Fig. 3*I*) compared to $Shfl^{+/+}$ control mice (Fig. 3*J*). Similar results were observed when mice were inoculated with a higher dose of ZIKV (*SI Appendix*, Fig. S5 *A–C*). These results indicate that $Shfl^{-/-}$ mice have a lethal phenotype at LD50 doses for $Shfl^{+/+}$ mice and demonstrate that *Shfl* plays a critical role in the controlling flavivirus-induced pathogenesis.

We also assessed the role of *Shfl* in a mouse model of alphavirus pathogenesis. Similar to the in vitro studies, in which alphaviruses were less inhibited by SHFL than flaviviruses (Fig. 1*D*), disease outcomes in $Shfl^{-/-}$ mice infected with SINV appeared minimal compared to $Shfl^{+/+}$ mice. Though the $Shfl^{-/-}$ mice appeared to be slightly more affected in terms of higher clinical scores, more severe weight loss, and decreased survival, these outcomes did not reach statistical significance (*SI Appendix*, Fig. S5 *D–F*).

To determine the contribution of virus-induced effects and host responses to the enhanced susceptibility of $Shfl^{-/-}$ mice to ZIKV, we performed a time course of infection and evaluated viral titers, tissue pathology, and systemic inflammatory responses. Liver, spleen, pancreas, spinal cord, and brain were harvested on days 3, 5, and 7 postinfection with ZIKV-Dakar 41519, and on day 6, serum cytokine levels were determined. Cytokine levels in infected $Shfl^{+/+}$ and $Shfl^{-/-}$ mice were not significantly different (*SI Appendix*, Fig. S6). Additionally, we found no significant differences in viral titers in spleen (Fig. 4*A*) and pancreas (Fig. 4*B*) or in relative ZIKV RNA levels in the liver (Fig. 4*C*) at any time point. However, ZIKV titers in the brain (Fig. 4*D*) and spinal cord (Fig. 4*E*), which peaked at the point of humane euthanasia, were significantly higher in $Shfl^{-/-}$ mice than $Shfl^{+/+}$ mice. On histopathology, we found no difference in inflammation of the liver (*SI Appendix*, Fig. S7 *A* and *D*) or spleen (*SI Appendix*, Fig. S7 *B* and *E*), as scored by a blinded, independent pathologist. In contrast, we found significantly more inflammation in the cerebral cortex of $Shfl^{-/-}$ mice (Fig. 4*F*) and a trend toward more necrosis in the hippocampus (Fig. 4*G*) and inflammation in the spinal cord (Fig. 4*H*). The increased inflammation in $Shfl^{-/-}$ mice (Fig. 4*I*) compared to $Shfl^{+/+}$ mice (Fig. 4*J*) was evident in the forms of increased perivascular inflammation in the cortex, increased pyknosis and cell death in the hippocampus, and increased inflammation of the meninges (black circles) and spinal cord (*SI Appendix*, Fig. S7 *C* and *F*). The observed increase of both inflammation and ZIKV titers in the brain and spinal cord of $Shfl^{-/-}$ mice, without a rise in serum cytokines, suggests that the cause of lethality in the $Shfl^{-/-}$ mice is likely due to exacerbated viral replication in the central nervous system rather than a detrimental systemic immune response to the infection.

To examine how viral burden correlates with Shfl expression in the infection model, we assessed Shfl expression in the brain, spinal cord, liver, and spleen of infected $Shfl^{+/+}$ and $Shfl^{-/-}$ mice (*SI Appendix*, Figs. S8 and S9). Despite Ifnar1 blockade, wild-type mice still express Shfl, indicating that Shfl in certain tissues may be both an ISG effector and a constitutively expressed restriction factor, which is supported by single-cell RNA-sequencing data in mice (38). Thus, in this ZIKV model, Ifnar1 blockade likely establishes an innate immunodeficiency in which constitutively expressed Shfl becomes a critical neuroprotective factor in the absence of classical ISG induction.

Discussion

Our studies and others have shown that SHFL is an ISG that is potently antiviral across the *Flaviviridae* (25–28). Inhibition mechanisms supported by these studies have varied, but the RNA-binding potential of SHFL has been demonstrated here as well as by previous studies (25, 26, 28, 30). SHFL-mediated restriction of DENV has been proposed to be mediated by inhibition of translation or by degradation of viral genomes in P bodies (25, 26). Lysosomal degradation of ZIKV NS3 has also been implicated as a mechanism for SHFL (28). In a study on HCV, SHFL impaired HCV replication organelle formation, and this was associated with lowered phosphatidylinositol-4-phosphate [PI(4)P] levels (27). Our mechanistic findings are largely consistent with those of Kinast et al. and together strongly suggest that SHFL inhibits viral genome replication and not primary translation of the incoming genome (27). Additional studies are needed to assess further post-primary translation mechanisms of SHFL action.

Outside of the *Flaviviridae*, SHFL has also been shown to inhibit HIV-1 by suppressing −1 programmed ribosomal frameshifting (−1PRF), which is required for optimal ratios of viral gag and gag-pol production (30, 39). This mechanism is consistent with our early observation that SHFL expression was incompatible with lentivirus production, which led to the plasmid-based screening strategy presented in this study. Coronaviruses use −1PRF to express the two major viral polyproteins (40, 41). However, ectopic expression of SHFL inhibited neither HCoV-OC43 nor SARS-CoV-2. −1PRF has been implicated in the alternative translation of NS1′ in some flaviviruses. However, this protein is thought to contribute more to pathogenesis in vivo rather than the viral replication cycle (42). Another study found that during HCV infection, −1PRF is not a primary mechanism of viral inhibition for SHFL (27). Taken together, our work and previous studies indicate that mechanisms unrelated to −1PRF may be contributing to SHFL-

mediated suppression of flavivirus replication. It is also unclear how SHFL and PRF impact alphaviruses. Our studies and others have shown that in vitro, SHFL inhibits VEEV and SINV (30). However, our in vivo studies with SINV in *Shfl*$^{-/-}$ mice thus far do not demonstrate that SHFL-mediated inhibition of SINV translates to protection from clinical disease (*SI Appendix*, Fig. S5 *D–F*). This contrasts with in vivo studies of −1PRF ablated VEEV, wherein neuropathogenicity was impaired (43). As stated earlier, while −1PRF does not seem to be as pivotal in the *Flaviviridae* replication cycle as for HIV, there is a suggested role for NS1′, the −1PRF protein encoded within NS2A, in neuroinvasiveness of the Japanese encephalitis virus serogroup, such as WNV (44, 45). Whether SHFL controls neuroinvasiveness of Zika or other flaviviruses by inhibiting −1PRF is an interesting area for future research.

In this report of virus infection in a *Shfl* KO mouse, we show that *Shfl* protects mice from ZIKV-induced pathogenesis. The antiviral phenotype of human SHFL is conserved in the mouse ortholog and is important for restricting ZIKV replication in the brain and spinal cord. We speculate that this pathogenesis specificity is due to antiviral ISG redundancy in noncentral nervous system (CNS) tissues relative to CNS. Indeed, disease and lethality in *Shfl*$^{-/-}$ mice appears to be predominantly mediated by encephalitis due to excess viral burden rather than hepatitis, pancreatitis, or host-induced immunopathology. Notably, since tissue expression was determined in the absence of infection/stimulation, and since we used Ifnar1 blockade for the infection model, our results suggest that *Shfl* likely has a role in this model as a cell intrinsic restriction factor independent of IFN signaling. Thus, while SHFL is a bona fide ISG, further examination of the role in IFN-induced SHFL will require immunocompetent mouse models that do not require IFN blockade.

Beyond these findings, additional targeted studies will be needed to determine which regions of the brain and which cell types are most impacted by the loss of *Shfl* in ZIKV-infected mice. We are also interested in determining whether *Shfl* controls other RNA viruses in vivo, as the antiviral specificity of this effector is quite broad. Lastly, the role of SHFL during neurotropic flavivirus infection in humans needs to be examined by infection studies in relevant primary neuronal cell cultures and by gene expression/correlation studies in primary human tissue samples. Such future studies will help define the role of this critical antiviral gene during mammalian infection with pathogenic flaviviruses.

Materials and Methods

Ethics Statement. All procedures used in this study complied with federal and institutional guidelines enforced by the University of Texas Southwestern Medical Center (UTSW) Institutional Animal Care and Use Committee (IACUC) and were granted institutional approval after veterinary and committee review. Animal studies were conducted under UTSW IACUC protocol no. 2016-101828. All available measures to maintain humane conditions were adhered to minimize suffering of the animals.

Mice. *Shfl*$^{+/-}$ mice on a C57BL/6J background were obtained from the University of California, Davis/KOMP (Knockout Mouse Project). Heterozygous *Shfl* mice were crossed to obtain *Shfl*$^{-/-}$ mice. *Shfl*$^{-/-}$ or *Shfl*$^{+/+}$ C57BL/6J littermates were used for a majority of experiments when possible; otherwise, mice of a similar age (within 1 wk) were used. Sample size was chosen based on published studies, and no randomization or blinding was performed aside from the scoring of histology. Genotype was confirmed by PCR of genomic DNA in house or outsourced to Transnetyx. Ablation of *Shfl* was confirmed by qPCR in spleen, liver, and brain, as well as by Western blot in multiple tissues. Animal studies were carried out in specific pathogen-free barrier facilities managed and maintained by the UTSW Animal Resource Center. Facilities were maintained at an acceptable range of 68 to 79 °F at a humidity of 30 to 70% on a 12-h dark/12-h light cycle.

In Vivo Infection, Viral Titers, and Organ Histology. Female and male mice (4 to 5 wk old) were injected intraperitoneally with ZIKV-MR766, ZIKV-Dakar 41519, or SINV-A300 diluted in phosphate-buffered saline (PBS) to the indicated titers or PBS for a mock infection control. *Shfl*$^{+/+}$ mice were used for infection controls. For ZIKV infections, mice were injected either with a single dose of 2 mg *Ifnar* antibody, MAR1-5A3 on day −1 (Fig. 3 *C* and *D*) or alternatively, on day −1, day +1, and day +4 relative to infection day, with 2 mg, 0.5 mg, and 0.5 mg anti-mouse *Ifnar* antibody, MAR1-5A3 (Figs. 3 *E–H* and 4), or when indicated, anti-human IFN-γ receptor antibody for control (Fig. 3 *C* and *D*). All infected mice were monitored daily for weight, morbidity, and mortality. Animals that were moribund or had lost more than 20% of their original body weight were euthanized per IACUC guidelines. At time of euthanasia, mice were saline perfused and organs were harvested. Viral titers in liver, pancreas, spleen, brain, and spinal cord were determined from freeze–thawed organs after weighing, homogenization, and plaque assay on baby hamster kidney cells. Relative viral titers, where indicated, were determined from freeze–thawed organs after storing in RNAlater at 4 °C for 1 to 28 d, followed by homogenization and RNA isolation using TRIzol (Invitrogen) (18). qRT-PCR was performed using QuantiFast SYBR Green PCR Kit (Qiagen) with a previously published pan-ZIKV primer set (46).

Livers, spleens, pancreas, brains, and spinal cords were fixed in 10% neutral buffer formalin, embedded in paraffin, sectioned at 5 μM, and stained with hematoxylin and eosin. Slides were analyzed by an independent pathologist (UTSW Animal Resource Center) who was blinded to the experimental conditions. A numerical score was assigned for the degree of inflammation for each brain and spinal cord and degree of necrosis for each hippocampus. Inflammatory cell infiltration was scored using the following criteria: 0 = none, 1 = minimal, 2 = mild, 3 = moderate, and 4 = marked. The necrosis score was defined by the percentage of necrosis (0 = none, 1 = <2%, 2 = 2 to 20%, 3 = 21 to 40%, and 4 = >40%).

Chemokine and cytokine analysis was conducted on serum that was collected 6 d postinfection with 250 plaque forming units (pfu) ZIKV-Dakar 41519. Serum was diluted 1:2 and was assayed per manufacturer's published protocol using Mouse Magnetic Luminex Assay (R&D Systems, catalog no. LXSAMSM-12).

Viruses and Cells.

Cells. Huh7.5, U-2 OS, HEK293T (from C. Rice, The Rockefeller University) cells, and all derivatives were maintained in Dulbecco's modified Eagle's medium (DMEM) supplemented with 10% fetal bovine serum (FBS) and 1× nonessential amino acids (NEAA). BHK21-J (from C. Rice) were grown in MEM supplemented with 10% FBS and 1× NEAA. Human *STAT1*$^{-/-}$ fibroblasts (from J.-L. Casanova, The Rockefeller University) were maintained in RPMI supplemented with 10% FBS and 1× NEAA. All media, FBS, and NEAA are from Gibco. Stable cells expressing antibiotic resistance genes were grown in complete media supplemented with puromycin (Sigma-Aldrich) at 2 μg mL^{-1}. Cell lines were routinely tested for mycoplasma contamination using the PCR-based Vendor GeM *Mycoplasma* Detection Kit (MP0025-1KT, Sigma-Aldrich). Cell lines were authenticated with short tandem repeat analysis using the ATCC Cell Line Authentication service.

Viruses. The following viruses and replicons were used in the preparation of this manuscript, with generation and propagation previously described (11, 47): YFV strain 17D expressing Venus GFP (YFV-Venus), HCV genotype 2a intragenotypic chimera expressing Ypet GFP (HCV-Ypet), CVB-GFP, nonreporter SINV A300, SINV expressing GFP (SINV-GFP), VEEV expressing enhanced GFP (VEEV-GFP) derived from the TC83 vaccine strain of VEEV (from I. Frolov), WNV-GFP, MV Edmonston lineage expressing GFP, HCV replicon expressing Gluc (Bi-Gluc-JFH-SG), and ZIKV strain PRVABC59 (48). HCV-Gluc was generated from the infectious clone Jc1FLAG(p7-nsGluc2A) as previously described (49). A ZIKV MR766-GFP infectious clone (provided by M. Evans, Icahn School of Medicine at Mount Sinai) was used to generate the virus as described previously (50). The infectious clone pACNR-FLYF-17Dx (C. Rice) was used to generate nonreporter YFV-17D as previously described (14). Virus-containing supernatants were collected, clarified by centrifugation, and stored at −80 °C. Human coronavirus OC43 (ATCC strain VR-1558) was propagated in HCT-8 cells as specified by the ATCC. Viral titers were determined by antibody staining (MAB9012, Millipore) and flow cytometry (51). SARS-CoV-2 (strain USA-WA1/2020) was obtained from the World Reference Center for Emerging Viruses and Arboviruses, University of Texas Medical Branch. Virus was propagated by low multiplicity of infection (MOI 0.01 to 0.001) in VeroE6 cells. When 70 to 90% cytopathic effect was observed (48 to 72 h postinfection), virus-containing supernatant was harvested, clarified by centrifugation, aliquoted, and stored at −80 °C until use. Viral titers were determined by TCID50 assay in VeroE6 cells.

Lentivirus and in vitro infections. Lentivirus production and transductions were performed as previously described (11). Viral infections for GFP-expressing reporter viruses, as well as nonreporter DENV and ZIKV, were conducted as previously described (11, 47, 48). SARS-CoV-2 and WNV infections

MICROBIOLOGY

were done in the BSL3 containment unit with approved conditions. For SARS-CoV-2 infections, stable Huh7.5 cells expressing SHFL or empty vector were infected with an MOI of 2. For the WNV ISG screen (Fig. 1*A*), HEK293T cells were plated at a density of 1×10^5 cells per 24 well in "complete" DMEM with 1× penicillin/streptomycin. Cells were transfected using XtremeGene 9 per manufacturer's protocol (Sigma-Aldrich, no. XTG9-RO) and incubated 24 h at 37 °C prior to infection with 5 MOI WNV-GFP. After approximately one viral replication cycle, cells were harvested for analysis by flow cytometry. Plotted in Fig. 1*A* are ISGs with transfection efficiency leading to harvest of at least 2,500 cells. Data for all 52 ISGs screened plus positive and negative controls (IRF1 and Fluc, respectively) are shown in *SI Appendix*, Table S1. For Fig. 1*C*, U2OS cells were transiently transfected with siRNA, as discussed in *siRNA-Mediated Gene Silencing*, prior to infection with YFV . For Fig. 1*D*, cells used for infections included empty vector or SHFL expressing stable Huh7.5 (WNV, VEEV, DENV, HCV, YFV, ZIKV, EAV, CVB, SINV, OC43, CoV2, VSV, PIV3, and MV) or stable $STAT1^{-/-}$ cells (ONNV, RSV, and IAV).

For the reporter HCV-Gluc growth curve, cells were infected with at least 1 MOI in DMEM supplemented with 1% FBS for 1 h. Media were aspirated, and cells were washed with serum-free DMEM four times and replaced with 500 μL complete DMEM. Supernatants were collected at specified time points and quantified by relative luciferase units by luminometry using Rluc assay system (Promega). Studies using the HCV subgenomic replicon (Bi-Gluc-JFH[SG]) and the polymerase-defective Bi-Gluc-JFH-GNN[SG] (HCV-GNN) were carried out as previously described (11). The YFV-17D subgenomic replicon YFV-Rluc (from R. Kuhn) was propagated, and viral RNA was generated as previously described (52). Assays to detect YFV-Rluc replicon activity were conducted similar to HCV replicon studies, with the detection of intracellular Rluc using the Renilla Luciferase Assay System (Promega).

siRNA-mediated gene silencing. SHFL siRNA (Thermo Fisher Scientific s30768) or Allstars Negative Control siRNA (Qiagen 1027280) at 20 nM was transfected into U2OS with HiPerfect Transfection Reagent (Qiagen) according to the manufacturer's reverse transfection protocol for 6-well plates. Cells were dissociated 48 hours post transfection and replated for infection in 24-well plates at a density of 5×10^4 cells per well and incubated overnight. The next day, cells were treated for 8 h with the indicated amounts of human IFN-α. Cells were then infected with 2.5 MOI YFV-17D-Venus for 1 h. Cells were harvested 48 h postinfection and analyzed by flow cytometry.

Antibody staining. Nonreporter virus infections were assessed using antibody staining targeting envelope protein (antibody D1-4G2-4-15, ATCC) for DENV and ZIKV infections as indicated. Cells were fixed in 4% paraformaldehyde in PBS for 20 min, permeabilized with 0.2% Triton X-100 in PBS for 5 min, and blocked with 10% bovine serum albumin for 30 min. Cells were incubated with primary antibody for 1 h at room temperature, followed by incubation in secondary antibody for 30 min at room temperature. Alexa Fluor–conjugated secondary antibody, AF-488 for green channels and AF-555 for red channels (Life Technologies) were used. Cells were mounted with ProLong Diamond with DAPI (Life Technologies) and imaged with a Zeiss Axiovert 200 microscope, unless otherwise indicated.

dsRNA. Approximately 20,000 Huh7.5 cells stably expressing HA.SHFL or an empty vector were plated into 8-well chamber slides. Cells were infected with 1 MOI YFV-17D for 1 h. Cells were incubated for 48 h and were stained with J2 anti-dsRNA antibody (1:500, Scions), following the protocol for antibody staining, mounting, and imaging as described in *Antibody Staining*..

Electron Microscopy. Approximately 2×10^6 Huh7.5 cells stably transduced with SCRPSY.empty or SCRPSY.SHFL lentivirus were seeded into 10-cm^2 tissue culture dishes. The next day, cells were either mock infected or infected with YFV-17D or HCV at 1 MOI. Cells were processed 24 h (YFV) or 48 h (HCV) postinfection for electron microscopy as previously described (48). Blocks were sectioned with a diamond knife (Diatome) on a Leica Ultracut UCT (7) ultramicrotome (Leica Microsystems) and collected onto copper grids. Images were acquired on a Tecnai G2 spirit transmission electron microscope (FEI) equipped with a LaB6 source using a voltage of 120 kV. Twenty cells of each cell line were reviewed, and representative images are shown.

Western Blots. For in vitro and in vivo protein expression assays, cells were either lysed directly and boiled in sodium dodecyl sulfate polyacrylamide gel electrophoresis (SDS-PAGE) sample buffer (100 mM Tris [pH 6.8], 20% glycerol, 4% SDS, 2% BME and 0.1% Bromophenol blue) or lysed in radioimmunoprecipitation assay (RIPA) buffer (containing 25 mM Tris [pH 7.5], 150 mM NaCl, 0.1% SDS, 0.5% sodium deoxycholate, 1% Triton X-100, and 1× Complete Protease Inhibitor Cocktail [Roche]) or in Nonidet P-40 lysis buffer (containing 50 mM Tris [pH 7.5], 150 mM NaCl, 1 mM EDTA, 1% Nonidet P-40, and 1× Complete Protease Inhibitor Cocktail). The protein concentration of cell lysates was determined by bicinchoninic acid (BCA) protein assay (Pierce Thermo Scientific). Lysates were separated on 12% polyacrylamide gels using the Laemmli method, and proteins were blotted to polyvinylidene difluoride membranes (Bio-Rad) and processed for Western blotting. Membranes were blocked in 5% milk in TBST (50 mM Tris-Cl [pH 7.5], 150 mM NaCl, and 0.05% Tween-20), followed by incubation with primary antibody for 1 to 1.5 h and secondary antibodies for 30 to 45 min. Proteins were visualized by incubating blots with enhanced chemiluminescent substrate (Pierce or Clarity, Bio-Rad) and exposing blots to autoradiography film (Denville Scientific). SHFL was detected using a polyclonal rabbit antibody [Sigma-Aldrich, HPA042001 or Protein-Tech, 27865-1-AP (in *SI Appendix*, Figs. S8 and S9)]. Loading control antibodies used in the study include the following: anti–β-actin (Abcam, ab6276), mouse monoclonal anti–β-actin-horseradish peroxidase (Sigma-Aldrich, A3854), or anti-GAPDH (Abcam, ab8245).

For mouse expression analysis (Fig. 3 and *SI Appendix*, Fig. S4), mice were humanely euthanized, perfused with heparinized saline, and organs removed. Organs were homogenized, and protein was isolated using RIPA buffer. Protein concentration was determined by BCA protein assay, and 30 μg protein was loaded per well, and gels were probed for *Shfl*. For each organ in Fig. 3, the first lane is the $Shfl^{+/+}$ mouse and the second lane is the $Shfl^{-/-}$ mouse. Positive control in final lane of upper left and lower blots is from HEK293T cells with ectopic expression of *Shfl*. For *SI Appendix*, Figs. S8 and S9, the mouse genotypes and days of harvest postinfection are as shown in figures.

CLIP. Cells were washed with PBS and cross-linked with 150 mJ/cm^2 in a Spectrolinker XL1000 (Spectroline). Cells were scraped, pelleted, and snap frozen. Cells were thawed and lysed in SDS lysis buffer (0.5% SDS, 50 mM Tris-Cl pH 6.8, 1 mM EDTA, 0.125 mg/mL heparin, 2.5 mg/mL torula yeast RNA [Sigma-Aldrich], and 1× protease inhibitors [Roche]). Samples were boiled at 65 °C for 5 min and returned to ice. Buffer was adjusted to RIPA buffer (1% Nonidet P-40, 0.5% sodium deoxycholate, 0.1% SDS, 150 mM NaCl, 50 mM Tris-Cl pH 8.0, 2 mM EDTA) by addition of a correction buffer (1.25% Nonidet P-40, 0.625% sodium deoxycholate, 62.5 mM Tris · HCl pH 8.0, 2.25 mM EDTA, 187.5 mM NaCl). Lysate was passed through a QIAshredder (Qiagen) twice. Lysates were cleared by three high-speed spins with tube transfers. Cleared lysates were supplemented with 5 mM CaCl2 and treated with 30 U of DNase (NEB) for 15 min. Antibody conjugated beads (preconjugated anti-HA) were added to samples (Pierce). Samples were rotated end over end at 4 °C for 2 h. Samples were placed on a magnetic separator and washed three times with RIPA, once with RIPA supplemented with 1 M Urea, and twice with RIPA. RNA was eluted from beads by addition of Proteinase K buffer (0.5 mg/mL Proteinase K [Ambion], 0.5% SDS, 20 mM Tris-Cl pH 7.5, 5 mM EDTA, 16.7 ng/μL GlycoBlue [Invitrogen], 0.1 mg/mL torula yeast RNA) and incubation for 1 h with shaking at 37 °C. Following elution, RNA was extracted with phenol-chloroform-isoamyl alcohol, extracted with chloroform, precipitated, DNase-treated, repurified, and complimentary DNA (cDNA) was generated using SuperScript IV and random hexamers. cDNA was treated with RNase H and RNase A, precipitated, and resuspended in a low volume of water for storage at −20 °C. cDNA was diluted prior to qPCR. Primers used are shown in *SI Appendix*, Table S5.

Statistics and reproducibility. Statistical analyses were performed with GraphPad Prism software. In all figures, the data points and bar graphs represent the mean of independent biological replicates. Except where noted, the error bars represent the SD and are only shown for experiments with $n = 3$ or greater, and the individual data points are overlaid. Western blots are representative of multiple biological replicates showing similar results. Uncropped blots are presented in *SI Appendix*, Figs. S4 and S9. Microscopy-based data are representative of multiple biological replicates showing similar results, as follows: immunofluorescence microscopy, $n = 3$ (Fig. 2*H*); and electron microscopy, $n = 3$ (Fig. 2 *I* and *J*). The histopathology was reviewed by a licensed veterinary pathologist who was blinded to the genotype of the mice. Two mice were omitted from analysis (one $Shfl^{+/+}$ and one $Shfl^{-/-}$) as qRT-PCR determined *Shfl* levels did not match their expected genotypes.

Data Availability. All study data are included in the article and/or *SI Appendix*.

ACKNOWLEDGMENTS. The mouse strain used for this research project was generated by the trans-NIH KOMP and obtained from the KOMP Repository (https://www.komp.org). The graphic in Fig. 3*G* was generated using Biorender.com. J.W.S. and N.W.H. thank technicians in the UTSW Animal Resource Center for their assistance and care and present and past members of the J.W.S. laboratory for their advice and feedback. This work was supported by the following NIH grants: K08AI132751 (N.W.H.), AI117922, and AI158124 (J.W.S.) and Training Grant AI005284 (K.B.M.). The generation of ES cells and KO mice by KOMP was supported in part by NIH Grants HG004085, HG004080, and RR024244. Additional grant support came from the Children's Health Clinical Research Advisory Committee, the W.W. Caruth Foundation (to N.W.H.), and a Burroughs Wellcome Fund "Investigators in the Pathogenesis of Infectious Disease" award (to J.W.S.).

1. T. C. Pierson, M. S. Diamond, The continued threat of emerging flaviviruses. *Nat. Microbiol.* **5**, 796–812 (2020).
2. Centers for Disease Control and Prevention (CDC), West Nile virus and other arboviral diseases - United States, 2012. *MMWR Morb. Mortal Wkly. Rep.* **62**, 513–517 (2013).
3. A. K. Pinto *et al.*, Deficient IFN signaling by myeloid cells leads to MAVS-dependent virus-induced sepsis. *PLoS Pathog.* **10**, e1004086 (2014).
4. B. L. Fredericksen, M. Smith, M. G. Katze, P. Y. Shi, M. Gale Jr., The host response to West Nile virus infection limits viral spread through the activation of the interferon regulatory factor 3 pathway. *J. Virol.* **78**, 7737–7747 (2004).
5. J. D. Brien *et al.*, Interferon regulatory factor-1 (IRF-1) shapes both innate and CD8(+) T cell immune responses against West Nile virus infection. *PLoS Pathog.* **7**, e1002230 (2011).
6. M. A. Samuel *et al.*, PKR and RNase L contribute to protection against lethal West Nile virus infection by controlling early viral spread in the periphery and replication in neurons. *J. Virol.* **80**, 7009–7019 (2006).
7. A. L. Brass *et al.*, The IFITM proteins mediate cellular resistance to influenza A H1N1 virus, West Nile virus, and dengue virus. *Cell* **139**, 1243–1254 (2009).
8. A. W. Bigham *et al.*, Host genetic risk factors for West Nile virus infection and disease progression. *PLoS One* **6**, e24745 (2011).
9. M. S. Suthar, M. S. Diamond, M. Gale Jr., West Nile virus infection and immunity. *Nat. Rev. Microbiol.* **11**, 115–128 (2013).
10. J. W. Schoggins, Interferon-stimulated genes: What do they all do? *Annu. Rev. Virol.* **6**, 567–584 (2019).
11. J. W. Schoggins *et al.*, A diverse range of gene products are effectors of the type I interferon antiviral response. *Nature* **472**, 481–485 (2011).
12. C. Li *et al.*, 25-hydroxycholesterol protects host against Zika virus infection and its associated microcephaly in a mouse model. *Immunity* **46**, 446–456 (2017).
13. R. C. Fleith *et al.*, IFIT3 and IFIT2/3 promote IFIT1-mediated translation inhibition by enhancing binding to non-self RNA. *Nucleic Acids Res.* **46**, 5269–5285 (2018).
14. R. B. Richardson *et al.*, A CRISPR screen identifies IFI6 as an ER-resident interferon effector that blocks flavivirus replication. *Nat. Microbiol.* **3**, 1214–1223 (2018).
15. K. Vonderstein *et al.*, Viperin targets flavivirus virulence by inducing assembly of non-infectious capsid particles. *J. Virol.* **92**, e01751-17 (2017).
16. S. V. Scherbik, J. M. Paranjape, B. M. Stockman, R. H. Silverman, M. A. Brinton, RNase L plays a role in the antiviral response to West Nile virus. *J. Virol.* **80**, 2987–2999 (2006).
17. A. I. Chiramel *et al.*, TRIM5α restricts flavivirus replication by targeting the viral protease for proteasomal degradation. *Cell Rep.* **27**, 3269–3283.e6 (2019).
18. I. N. Boys *et al.*, RTP4 is a potent IFN-inducible anti-flavivirus effector engaged in a host-virus arms race in bats and other mammals. *Cell Host Microbe* **28**, 712–723.e9 (2020).
19. M. J. Gorman, S. Poddar, M. Farzan, M. S. Diamond, The interferon-stimulated gene Ifitm3 restricts West Nile virus infection and pathogenesis. *J. Virol.* **90**, 8212–8225 (2016).
20. H. Cho, B. Shrestha, G. C. Sen, M. S. Diamond, A role for Ifit2 in restricting West Nile virus infection in the brain. *J. Virol.* **87**, 8363–8371 (2013).
21. A. A. Perelygin *et al.*, Positional cloning of the murine flavivirus resistance gene. *Proc. Natl. Acad. Sci. U.S.A.* **99**, 9322–9327 (2002).
22. S. V. Scherbik, K. Kluetzman, A. A. Perelygin, M. A. Brinton, Knock-in of the Oas1b(r) allele into a flavivirus-induced disease susceptible mouse generates the resistant phenotype. *Virology* **368**, 232–237 (2007).
23. T. M. Lucas, J. M. Richner, M. S. Diamond, The interferon-stimulated gene Ifi27l2a restricts West Nile virus infection and pathogenesis in a cell-type- and region-specific manner. *J. Virol.* **90**, 2600–2615 (2015).
24. R. Lindqvist, C. Kurhade, J. D. Gilthorpe, A. K. Överby, Cell-type- and region-specific restriction of neurotropic flavivirus infection by viperin. *J. Neuroinflammation* **15**, 80 (2018).
25. Y. Suzuki *et al.*, Characterization of RyDEN (C19orf66) as an interferon-stimulated cellular inhibitor against dengue virus replication. *PLoS Pathog.* **12**, e1005357 (2016).
26. C. A. Balinsky *et al.*, *IRAV* (*FLJ11286*), an interferon-stimulated gene with antiviral activity against dengue virus, interacts with MOV10. *J. Virol.* **91**, e01606-16 (2017).
27. V. Kinast *et al.*, C19orf66 is an interferon-induced inhibitor of HCV replication that restricts formation of the viral replication organelle. *J. Hepatol.* **73**, 549–558 (2020).
28. Y. Wu *et al.*, C19orf66 interrupts Zika virus replication by inducing lysosomal degradation of viral NS3. *PLoS Negl. Trop. Dis.* **14**, e0008083 (2020).
29. K. B. Mar *et al.*, LY6E mediates an evolutionarily conserved enhancement of virus infection by targeting a late entry step. *Nat. Commun.* **9**, 3603 (2018).
30. X. Wang *et al.*, Regulation of HIV-1 gag-pol expression by shiftless, an inhibitor of programmed -1 ribosomal frameshifting. *Cell* **176**, 625–635.e14 (2019).
31. W. Rodriguez, K. Srivastav, M. Muller, C19ORF66 broadly escapes virus-induced endonuclease cleavage and restricts Kaposi's sarcoma-associated herpesvirus. *J. Virol.* **93**, e00373-19 (2019).
32. A. E. Shaw *et al.*, Fundamental properties of the mammalian innate immune system revealed by multispecies comparison of type I interferon responses. *PLoS Biol.* **15**, e2004086 (2017).
33. W. C. Skarnes *et al.*, A conditional knockout resource for the genome-wide study of mouse gene function. *Nature* **474**, 337–342 (2011).
34. A. Grant *et al.*, Zika virus targets human STAT2 to inhibit type I interferon signaling. *Cell Host Microbe* **19**, 882–890 (2016).
35. K. C. Sheehan, H. M. Lazear, M. S. Diamond, R. D. Schreiber, Selective blockade of interferon-α and -β reveals their non-redundant functions in a mouse model of West Nile virus infection. *PLoS One* **10**, e0128636 (2015).
36. K. C. Sheehan *et al.*, Blocking monoclonal antibodies specific for mouse IFN-alpha/beta receptor subunit 1 (IFNAR-1) from mice immunized by in vivo hydrodynamic transfection. *J. Interferon Cytokine Res.* **26**, 804–819 (2006).
37. D. R. Smith *et al.*, Neuropathogenesis of Zika virus in a highly susceptible immunocompetent mouse model after antibody blockade of type I interferon. *PLoS Negl. Trop. Dis.* **11**, e0005296 (2017).
38. C. Tabula Muris *et al.*; Tabula Muris Consortium; Overall coordination; Logistical coordination; Organ collection and processing; Library preparation and sequencing; Computational data analysis; Cell type annotation; Writing group; Supplemental text writing group; Principal investigators, Single-cell transcriptomics of 20 mouse organs creates a Tabula Muris. *Nature* **562**, 367–372 (2018).
39. T. Jacks *et al.*, Characterization of ribosomal frameshifting in HIV-1 gag-pol expression. *Nature* **331**, 280–283 (1988).
40. E. P. Plant, J. D. Dinman, The role of programmed-1 ribosomal frameshifting in coronavirus propagation. *Front. Biosci.* **13**, 4873–4881 (2008).
41. M. Puray-Chavez *et al.*, The translational landscape of SARS-CoV-2 and infected cells. bioRxiv [Preprint] (2020). https://doi.org/10.1101/2020.11.03.367516 (Accessed 3 October 2021).
42. J. F. Atkins, G. Loughran, P. R. Bhatt, A. E. Firth, P. V. Baranov, Ribosomal frameshifting and transcriptional slippage: From genetic steganography and cryptography to adventitious use. *Nucleic Acids Res.* **44**, 7007–7078 (2016).
43. J. A. Kendra *et al.*, Ablation of programmed -1 ribosomal frameshifting in Venezuelan equine encephalitis virus results in attenuated neuropathogenicity. *J. Virol.* **91**, e01766-16 (2017).
44. E. B. Melian *et al.*, NS1′ of flaviviruses in the Japanese encephalitis virus serogroup is a product of ribosomal frameshifting and plays a role in viral neuroinvasiveness. *J. Virol.* **84**, 1641–1647 (2010).
45. W. J. Liu *et al.*, A single amino acid substitution in the West Nile virus nonstructural protein NS2A disables its ability to inhibit alpha/beta interferon induction and attenuates virus virulence in mice. *J. Virol.* **80**, 2396–2404 (2006).
46. A. M. Bingham *et al.*, Comparison of test results for Zika virus RNA in urine, serum, and saliva specimens from persons with travel-associated Zika virus disease - Florida, 2016. *MMWR Morb. Mortal. Wkly. Rep.* **65**, 475–478 (2016).
47. J. W. Schoggins *et al.*, Pan-viral specificity of IFN-induced genes reveals new roles for cGAS in innate immunity. *Nature* **505**, 691–695 (2014).
48. N. W. Hanners *et al.*, Western Zika virus in human fetal neural progenitors persists long term with partial cytopathic and limited immunogenic effects. *Cell Rep.* **15**, 2315–2322 (2016).
49. S. Marukian *et al.*, Cell culture-produced hepatitis C virus does not infect peripheral blood mononuclear cells. *Hepatology* **48**, 1843–1850 (2008).
50. M. C. Schwarz *et al.*, Rescue of the 1947 Zika virus prototype strain with a cytomegalovirus promoter-driven cDNA clone. *MSphere* **1**, e00246-16 (2016).
51. B. Grigorov, J. Rabilloud, P. Lawrence, D. Gerlier, Rapid titration of measles and other viruses: Optimization with determination of replication cycle length. *PLoS One* **6**, e24135 (2011).
52. C. T. Jones, C. G. Patkar, R. J. Kuhn, Construction and applications of yellow fever virus replicons. *Virology* **331**, 247–259 (2005).